PETAR: Localized Findings Generation with Mask-Aware Vision-Language Modeling for PET Automated Reporting

Danyal Maqbool¹, Changhee Lee¹, Zachary Huemann¹, Samuel D. Church¹, Matthew E. Larson¹, Scott B. Perlman¹, Tomas A. Romero¹, Joshua D. Warner¹, Meghan Lubner¹, Xin Tie¹, Jameson Merkow², Junjie Hu¹, Steve Y. Cho¹, Tyler J. Bradshaw¹

¹University of Wisconsin–Madison, Madison, WI, USA, ²Microsoft, Redmond, WA, USA

Abstract

Recent advances in vision-language models (VLMs) have enabled impressive multimodal reasoning, yet most medical applications remain limited to 2D imaging. In this work, we extend VLMs to 3D positron emission tomography/computed tomography (PET/CT)—a domain characterized by large volumetric data, small and dispersed lesions, and lengthy radiology reports. We introduce a large-scale dataset comprising over 11,000 lesion-level descriptions paired with 3D segmentations from more than 5,000 PET/CT exams, extracted via a hybrid rule-based and large language model (LLM) pipeline. Building upon this dataset, we propose PETAR-4B, a 3D mask-aware vision-language model that integrates PET, CT, and lesion contours for spatially grounded report generation. PETAR bridges global contextual reasoning with fine-grained lesion awareness, producing clinically coherent and localized findings. Comprehensive automated and human evaluations demonstrate that PETAR substantially improves PET/CT report generation quality, advancing 3D medical vision-language understanding.

1. Introduction

Vision—language models (VLMs) have recently achieved remarkable progress in aligning visual understanding with natural language generation, enabling powerful cross-modal reasoning across diverse domains. In the medical imaging field, 2D VLMs have shown promise in radiology report generation, potentially leading to accelerated clinical workflows and reduced radiologist burnout [9]. However, current medical VLM research has predominantly focused on 2D imaging modalities—such as chest X-rays or individual computed tomography (CT) slices—while 3D modalities, such as CT, magnetic resonance (MRI), and positron emission tomography (PET) have proven more challenging. This challenge arises not only from the substantially larger and more complex input data, but also from the substantially greater

length and complexity of the radiologist's reports, which can cover multiple anatomical regions and include numerous findings.

Of the 3D imaging modalities, PET is severely underrepresented in medical VLM research. PET imaging plays a critical role in oncology, including for diagnosis, staging, and treatment response assessment, and it is experiencing rapid growth in terms of imaging volumes. PET presents several unique challenges to traditional multimodal learning, including lower number of annual scans compared to other modalities, limited availability of public multimodal datasets, whole-body imaging volumes that demand large-scale 3D processing, and small but numerous lesion sites dispersed across scans. Moreover, PET reports are arguably the lengthiest reports in radiology, and can be 3 times longer than CT reports. These factors make PET interpretation particularly difficult for both conventional models and modern large-scale vision—language systems.

Recent works have demonstrated strong performance in PET lesion segmentation (e.g., AutoPET) and there is significant progress in large language models (LLMs) for structured text generation. However, a critical gap remains in connecting these segmentations with grounded, localized lesion descriptions. To address this, our work establishes a direct connection between the spatially localized lesion information and the corresponding textual findings. We rely on segmentations to produce these findings, which can be obtained from the aforementioned models or from point-and-click frameworks such as PET-Edge on MIM. Our contributions can be summarised as follows:

- We introduce a large-scale PET/CT dataset comprising 11,356 lesion descriptions paired with 3D segmentations from over 5,000 exams. This dataset, the first of its kind, uniquely links PET/CT lesions with descriptive referring expressions extracted from clinical reports using a hybrid pipeline of rule-based filters and LLMs.
- We develop a novel 3D mask-aware VLM, PETAR-4B, capable of jointly processing PET, CT, and lesion masks to produce localized, clinically meaningful findings. By



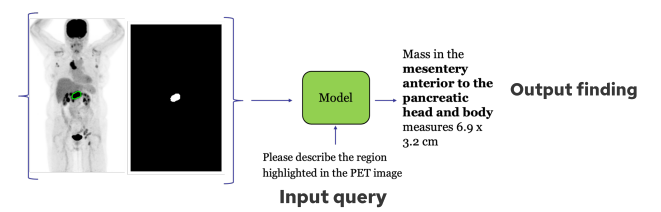


Figure 1. An example of mask guided response generation. We want the model to leverage the contour of the volume to generate grounded responses.

integrating 3D contour information into the visual encoder, PETAR effectively bridges global contextual reasoning with fine-grained lesion awareness.

We conduct a comprehensive evaluation of 2D and 3D vision—language models for PET findings generation, using both automated and human assessments to measure the quality of the generated texts and benchmark common metrics to identify the most reliable ones.

Through these contributions, PETAR advances the frontier of medical vision—language modeling by explicitly incorporating 3D PET understanding and mask-guided reasoning. This research was conducted under a protocol approved by our Institutional Review Board (IRB), which granted a waiver of informed consent. All data was fully anonymized prior to use.

2. Related Work

2.1. Medical Vision Language Models (VLMs)

Medical VLMs aim to bridge visual and textual modalities by encoding multimodal inputs—such as medical images and textual prompts—into a shared embedding space, and leveraging large language models to generate clinically meaningful outputs. Recent studies have explored diverse strategies within this paradigm. MAIRA [2, 11] generates detailed radiology reports from chest X-rays through aligned vision—language encoders, while LLaVA-Med [12] adapts general-domain VLMs to biomedical applications via curriculum learning on figure—caption pairs. However, these methods are limited to the 2D plane, discarding critical spatial information inherent in 3D medical volumes.

To extend multimodal reasoning into volumetric contexts, M3D [1] leverages a large-scale multimodal dataset for 3D segmentation and report generation. Merlin [3] aligns 3D CT data with both structured and unstructured clinical information within a unified embedding space, and CT2Rep [7] introduces a causal 3D feature extractor for automated chest CT report generation. RadFM [16], trained on both 2D and 3D data, seeks to build a generalist model capable of handling diverse radiologic tasks across modalities. While

these works mark substantial progress toward comprehensive 3D understanding, they remain *mask-agnostic*, limiting their ability to localize and describe specific lesions or regions with fine-grained precision. In contrast, our work introduces explicit mask-aware conditioning, enabling localized PET/CT report generation that bridges global volumetric reasoning with lesion-level granularity.

2.2. Fine-Grained Captioning

Significant advances have also been made toward finegrained visual grounding in 2D images. Early methods incorporate explicit spatial cues—such as bounding box coordinates—into textual prompts to direct visual attention [5, 14, 18]. More recent approaches have introduced flexible region-level interactions, allowing segmentation masks or point-based cues to guide the model's focus and improve spatial grounding [4, 8, 15, 17].

In the medical domain, Reg2RG [6] extends this idea by introducing a mask input channel to generate more detailed, region-aware findings from CT scans. However, its scope remains limited to chest CT imaging, without extending to other body regions or additional imaging modalities. Our work builds upon this direction by introducing a 3D, mask-aware architecture capable of integrating metabolic and anatomical cues, thereby enabling localized and clinically grounded captioning across full-body PET/CT volumes.

Table 1. Comparison of selected models on medical imaging modalities.

Model	3D	Mask-aware	CT	PET
ViP-LLaVA	×	✓	×	X
GLAMM	×	\checkmark	X	\checkmark
M3D	\checkmark	×	\checkmark	×
RadFM	\checkmark	×	\checkmark	×
CT2Rep	\checkmark	×	\checkmark	×
Med3DVLM	\checkmark	×	\checkmark	×
M3D-RAD	\checkmark	×	\checkmark	×
Reg2RG	\checkmark	\checkmark	\checkmark	×
PETAR (ours)	\checkmark	\checkmark	\checkmark	\checkmark

3. Dataset Construction

3.1. Preliminaries on PET/CT Reports

PET reports describe how radiotracers are distributed in the body, usually alongside CT or MRI imaging for anatomical reference. PET scans often cover all major body regions (head-to-thighs or head-to-feet) and are widely used in oncology. Within each body region, reports list the lesions or regions with abnormal radiotracer uptake and include measurements such as standardized uptake value (SUV_{max}), slice

numbers, and qualitative descriptions. Because lesions are usually tracked across multiple scans, these measurements and descriptions help future readers identify the lesions of concern. PET reports are written in free text and can vary in length. Moreover, reporting styles differ substantially between physicians and institutions. Two physicians describing the same lesion may use substantially different terminology (e.g., 'hypermetabolic,' 'hot,' 'high uptake,' 'tracer-avid') and levels of detail. Such non-uniformity creates a major challenge for automated PET reporting, a challenge further exacerbated by the scarcity of large-scale, annotated datasets, that are visually grounded.

To address this, we develop a pipeline that extracts structured lesion-level information from unstructured PET/CT reports.

3.2. Dataset Construction Pipeline

We build on the work developed by Huemann et al. [10]. Starting from nearly one million sentences in a dataset of clinical PET reports, we use this multi-stage pipeline to identify sentences mentioning both a slice number and an SUV_{max} value—key indicators that radiologists use when describing lesions. Our approach combines rule-based pattern matching, RadGraph (for anatomical term extraction), and large language model (LLM) ensembles (Mistral-7B-Instruct, Mixtral-8×7B-Instruct, and Dolphin-Instruct). These models filter out irrelevant sentences, disambiguate references to prior studies, and accurately extract the SUV_{max} and corresponding slice number. To generate lesion masks, we employ an iterative thresholding algorithm on the PET volume. The process begins by applying a dynamic threshold based on the reported SUV_{max}, producing an initial set of candidate regions. Connected components are then identified, and the component whose SUV_{max} matches the reported SUV_{max} (within ± 0.1) and intersects the reported axial slice is selected. This region is refined through adaptive thresholding, progressively removing background uptake while preserving the lesion core until the contour stabilizes.

The resulting dataset contains 11,356 lesion descriptions across 5,126 unique exams, covering multiple radiotracers including $^{18}\text{F-fluorodeoxyglucose}$ (FDG), $^{68}\text{Ga-(DOTA-(Tyr}^3)-octreotate)}$ (DOTATATE), $^{18}\text{F-fluciclovine}$, and $^{18}\text{F-DCFPyL}$. All PET, CT, and segmentation volumes were resampled to 3 mm isotropic resolution, and standardized to a fixed dimension of $192\times192\times352$ voxels.

To enhance textual consistency, we further processed each lesion description using an LLM (Qwen3-30B-A3B) that formats free-text sentences into a structured schema: region, organ, anatomic subsite, report. This representation makes spatial and anatomical references explicit, simplifying downstream grounding between the text and the 3D image, and simplifying performance evaluation. An example is shown in Fig. 2.



Figure 2. An example of our enhanced data format.

Finally, to improve the model's understanding of global anatomy, we curate a complementary pretraining dataset. We apply TotalSegmentator to our CT volumes to generate approximately 5,000 segmentations across its 117 predefined anatomical classes, providing broad coverage of structural features for volumetric pretraining.

Ours is the first publicly available multimodal PET/CT dataset with lesion-level granularity. As we highlight in Table 2, existing PET/CT datasets are typically limited in scope, focusing on specific organs, lacking text, lesion-level findings, or missing segmentation masks. In contrast, our dataset, PETAR-11K, provides the first large-scale, whole-body PET/CT collection with aligned findings, 3D lesion masks, and textual descriptions, enabling comprehensive volumetric understanding and report generation.

Table 2. Comparison of PET/CT datasets available

Dataset	3D CT	3D PET	Findings	Masks	Whole body
RIDER Lung PET-CT	✓	✓	×	×	×
Head-Neck PET-CT	\checkmark	\checkmark	×	×	×
Lung-PET-CT-Dx	\checkmark	\checkmark	×	×	×
FDG-PET-CT-Lesions	\checkmark	\checkmark	×	\checkmark	✓
SegAnyPet	×	\checkmark	×	\checkmark	✓
Pet2Rep	×	\checkmark	\checkmark	×	✓
ViMed-PET	\checkmark	\checkmark	\checkmark	×	✓
PETAR-11K (ours)	\checkmark	\checkmark	✓	\checkmark	✓

At the time of this submission, Pet2Rep and ViMed-PET have not made public their datasets, and so we do not use them in our evaluations.

4. Model Architecture

In this section, we present the proposed architecture to achieve that goal and outline the inputs utilized to generate detailed, localized findings for lesions.

4.1. Mask Aware Inputs

Given a PET scan $P \in \mathbb{R}^{D \times W \times H}$, a CT scan $C \in \mathbb{R}^{D \times W \times H}$, and a binary mask $M \in \{0,1\}^{D \times W \times H}$ indicating the region of interest, the objective is to generate detailed

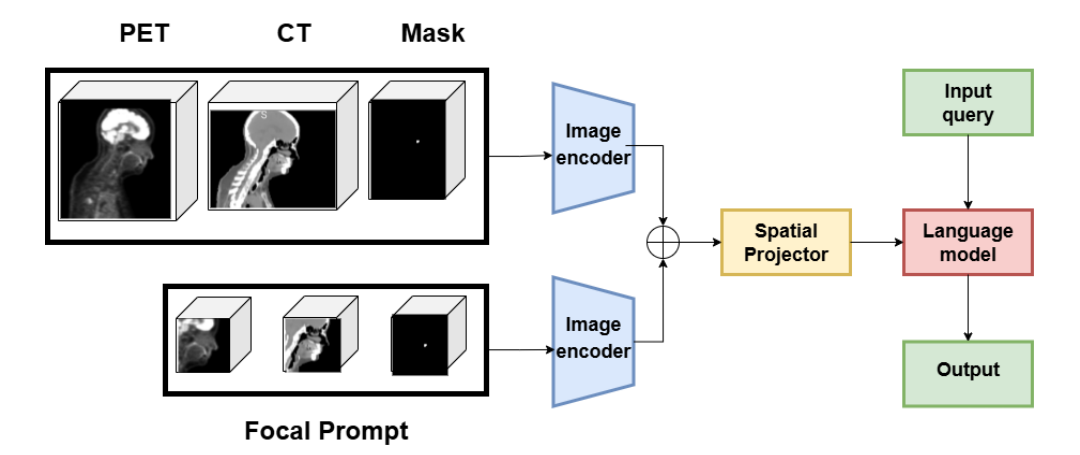


Figure 3. Overall architecture of the proposed method. The pipeline integrates PET, CT, and lesion mask inputs via convolutional layers and an M3D-CLIP encoder, followed by token fusion and spatial pooling. The pooled visual tokens are processed by a Phi-3B language model, which generates clinically grounded text reports conditioned on visual features and textual queries.

diagnostic findings restricted to the masked region. Let f_{θ} denote our model parameterized by θ . The formulation is as follows:

$$y = f_{\theta}(\boldsymbol{P}, \boldsymbol{C}, \boldsymbol{M})$$

4.2. Focal Prompt

A core issue of lesion-level understanding is that lesions are often a very small part of a volume, and so standard approaches lead to a risk of information loss during common global processing steps, such as resizing or cropping. For instance, in our dataset, the average lesion occupies less than 1% of the total scan volume. To address this, we introduce a 3D focal prompt to provide a localized, high-resolution view of the lesion, similar to prior work [8, 13].

We first center the crop around the mask M and extract a cubic subvolume encompassing the region of interest. To improve robustness and avoid overfitting to fixed spatial positions, we apply random spatial perturbations to both the cube center and its side length, with deviations constrained to 20% of the original mask center and cube size. The crop is adjusted such that the mask remains fully contained within the subcube, ensuring complete lesion visibility in the focal prompt.

Let the lesion mask centroid be $c_M \in \mathbb{R}^3$ and the desired crop size be r. We introduce small random perturbations to both the center and size to improve robustness:

$$\tilde{c} = c_M + \delta_c, \quad \tilde{r} = r + \delta_r,$$

$$\delta_c, \, \delta_r \stackrel{\text{i.i.d.}}{\sim} \mathcal{U}(-0.2r, 0.2r).$$

The focal PET, CT, and mask crops are then extracted as:

$$\mathcal{F}_P, \mathcal{F}_C, \mathcal{F}_M = \text{Crop}(\boldsymbol{P}, \boldsymbol{C}, \boldsymbol{M}; \tilde{c}, \tilde{r}),$$

where $\mathcal{F}_{\mathcal{P}}, \mathcal{F}_{\mathcal{C}}, \mathcal{F}_{\mathcal{M}}$ represent the PET, CT, and mask focal crops, and $Crop(\cdot)$ denotes the operation that extracts the 3D subvolume.

4.3. Shared Visual Encoding

We adopt a shared 3D vision transformer to encode both PET and CT volumes. Specifically, to prepare the sequential inputs for the shared transformer, we split the PET and CT volumes into non-overlapping 3D patches of size (s_D, s_W, s_H) , which are then flattened into a sequence of K patches, denoted as P_{patch} , $C_{\text{patch}} \in \mathbb{R}^{K \times s_D \times s_W \times s_H}$. We then linearly project the patches into the token embeddings.

$$Z_p = \text{PatchEmbed}(P) \in \mathbb{R}^{K \times d}$$
 (1)

$$\mathbf{Z}_C = \text{PatchEmbed}(\mathbf{C}) \in \mathbb{R}^{K \times d}$$
 (2)

We further encode the PET and CT patches using the shared 3D vision transformer \mathcal{T} , while incorporating the lesion mask via additive conditioning:

$$\mathbf{X}_{PET} = \mathcal{T}(\mathbf{Z}_P + \text{MaskEmbed}(\mathbf{M})), \ \mathbf{X}_{CT} = \mathcal{T}(\mathbf{Z}_C).$$
(3)

The two representations are fused by concatenating both the CT and mask-aware PET tokens along the embedding dimension:

$$\mathbf{X} = \operatorname{Concat}(\mathbf{X}_{PET}, \mathbf{X}_{CT}).$$

The same process is applied to focal crops $(\mathcal{F}_P, \mathcal{F}_C, \mathcal{F}_M)$, producing focal embeddings $\tilde{\mathbf{X}}$. Global and focal features are then combined via element-wise addition and reduced via spatial pooling [1]:

$$\mathbf{T} = (\mathbf{X} + \tilde{\mathbf{X}}) \in \mathbb{R}^{K \times d_v}.$$

These pooled tokens are linearly projected into the language model space:

$$\mathbf{V} = \text{Proj}(\text{SpatialPooler}(\mathbf{T})).$$

Finally, the projected tokens V and a lesion-description query q are passed to the language model decoder to generate localized findings:

$$y = \text{LMDecoder}(q, \mathbf{V}).$$

4.4. Training

We adopt a four-stage training pipeline designed to progressively align mask-aware PET/CT representations with the language model for lesion-focused report generation.

Stage 1: Pretraining. We begin by pretraining the model on the curated TotalSegmentator dataset, framing the region classification task as a text generation problem. Each sample is presented as a question—answer pair following the template: *Question:* "What is the region highlighted by the mask?" *Answer:* "The highlighted region is the < Region Class>." Multiple prompt variations are used to encourage linguistic diversity and generalization (details provided in the supplementary material).

Stage 2: Mask Embedding Alignment. In this stage, the mask embedding module is trained independently to align binary mask features with corresponding 3D anatomical structures. All other components remain frozen, allowing the model to learn robust mask-to-anatomy correspondences.

Stage 3: Projector Alignment. The projection head is then optimized to map mask-aware visual embeddings into the language model's feature space. During this phase, both the vision backbone and the LLM are frozen to ensure the projector learns semantically consistent cross-modal alignment between visual and textual representations.

Stage 4: Full Finetuning. Finally, the entire network is finetuned end-to-end on our region-aware PET/CT dataset. This stage enables the model to jointly refine all components for generating detailed, clinically grounded, and lesion-specific findings conditioned on the input mask.

4.5. Training Objective

The model is trained using an autoregressive negative loglikelihood objective conditioned on the visual inputs and preceding text tokens:

$$\mathcal{L} = -\sum_{\mathcal{D}} \sum_{i=1}^{N} \log p(y_i \mid \mathbf{V}, q, y_{< i}),$$

where \mathcal{D} denotes the training dataset, N is the number of tokens in each generated sequence, \mathbf{V} represents the visual tokens projected from the PET–CT–mask encoder, q is the lesion-description query, and y_i is the i^{th} language token in the generated report.

5. Experiments and Analysis

5.1. Implementation details

We adopt the vision encoder and language model from M3D, a popular baseline for medical VLMs as it has been trained on a large corpra of 3D medical images and corresponding text. All experiemnts are conducted on 2 NVIDIA L40S GPU. Stage 1 is trained for 5 epochs and all subsequent stages are trained for 10 eopchs. Training in total takes \sim 20 hours. A detailed list of hyperparameters can be found in our supplamnetary material.

5.2. Evaluation

Compared Models We include 2D VLMs, 2D prompt-aware VLMs, 3D VLMs, and 3D prompt-aware VLMs to ensure broad modality and capability coverage. For 2D VLMs, we select strong medical baselines including InternVL3-8B, Hautuo-7B, MedGemma-4B, and Qwen3-8B, each trained on large-scale medical and general-domain corpora. As 2D prompt-aware baselines, we evaluate ViP-LLaVA, which integrates visual grounding with mask-conditioned prompting. Among 3D VLMs, we benchmark against M3D, Med3DVLM, and M3D-RAD, all capable of volumetric reasoning on CT. Finally, we compare against 3D promptaware frameworks such as **Reg2RG** and our proposed model, which explicitly incorporates mask-guided conditioning. We also finetune representative models using our dataset for a fairer comparison and validation of our model architecture. We choose the best performing models in each category for further finetuning.

Metrics. To comprehensively evaluate model performance, we adopt multiple categories of metrics:

- **NLP Metrics:** BLEU, ROUGE, METEOR, and CIDEr. These metrics are widely used in prior works. They all measure n-gram overlap.
- Semantic Metrics: BERTScore and BARTScore, computed using checkpoints fine-tuned on large radiology corpora, to capture latent contextual similarity between predicted and reference reports.
- Language Model Metrics: RaTEScore and GREEN, which assess clinical plausibility and reasoning quality via language-model-based evaluation.

5.3. Human Evaluation

Automated evaluation metrics often fail to capture the nuanced clinical reasoning and linguistic preferences of radiologists. To address this limitation, we conducted two rounds of human-centered evaluations tailored to PET report generation.

In the first round, 100 pairs of ground-truth and modelgenerated findings were rated by board-certified physicians using our standardized scoring scheme. We then computed the Spearman's correlation between the automated metrics and the average human scores.

In the second round, we performed a larger physician-led evaluation on a stratified subset of the test set. A team of five board-certified nuclear medicine physicians assessed each report for *interpretation correctness*, *localization fidelity*,

Model	BLEU	ROUGE-L	METEOR	CIDEr	BART	BERT	RaTE	GREEN	
2D VLMs	2D VLMs								
Gemma	0.124	0.352	0.358	0.027	-4.92	0.690	0.540	0.011	
Hautuo	0.130	0.350	0.357	0.024	-4.85	0.695	0.584	0.015	
InternVL3	0.137	0.355	0.356	0.035	-4.72	0.694	0.614	0.030	
Qwen3	0.116	0.342	0.364	0.035	-4.83	0.696	0.531	0.013	
2D mask-aware VLMs	2D mask-aware VLMs								
ViP-LLaVA	0.064	0.301	0.308	0.009	-5.96	0.651	0.503	0.006	
3D VLMs	3D VLMs								
Med3DVLM	0.004	0.080	0.066	0.005	-5.7	0.511	0.285	0.002	
M3D	0.327	0.276	0.323	0.013	-5.32	0.634	0.505	0.000	
M3D-RAD	0.343	0.300	0.340	0.016	-5.23	0.658	0.518	0.003	
M3D-RAD (finetuned)	0.485	0.446	0.501	0.132	-4.34	0.750	0.627	0.071	
3D mask-aware VLMs									
Reg2RG	0.044	0.060	0.108	0.001	-5.540	0.518	0.363	0.002	
Reg2RG (finetuned)	0.478	0.416	0.487	0.055	-4.58	0.732	0.532	0.031	
PETAR-4B (Ours)	0.531	0.519	0.557	0.415	-4.04	0.791	0.708	0.246	

Table 3. Comparison of selected models on medical imaging modalities using multiple evaluation metrics.

Mask	CT	Focal	TS	BLEU	ROUGE	METEOR	CIDEr	BERTScore	BARTScore	RaTEScore	GREEN
×	×	X	×	-	-	-	-	-	-	-	-
×	×	×	\checkmark	0.485	0.446	0.501	0.132	0.750	-4.34	0.627	0.071
\checkmark	×	×	\checkmark	0.480	0.445	0.498	0.137	0.748	-4.33	0.626	0.088
×	\checkmark	×	\checkmark	0.477	0.436	0.499	0.134	0.746	-4.31	0.622	0.060
×	×	\checkmark	\checkmark	0.528	0.518	0.550	0.397	0.787	-4.05	0.698	0.226
\checkmark	×	\checkmark	\checkmark	0.525	0.518	0.550	0.381	0.787	-4.05	0.700	0.232
×	\checkmark	\checkmark	\checkmark	0.517	0.507	0.540	0.428	0.784	-4.08	0.587	0.234
	\checkmark	\checkmark	\checkmark	0.531	0.519	0.557	0.415	0.791	-4.04	0.708	0.246

Table 4. Ablation study of our model showing the effect of each component on multiple evaluation metrics.

Metric	Spearman's ρ
GREEN	0.608
ROUGE	0.470
RaTEScore	0.447
BERTScore	0.398
CIDEr	0.384
METEOR	0.362
BARTScore	0.313
BLEU	0.304

Table 5. Spearman's correlation between automated metrics and human evaluation scores. Higher correlation indicates stronger alignment with expert judgment.

and *clinical utility*. Each expert evaluated a sample of 16 lesions from 8 patients, providing detailed qualitative feedback alongside quantitative ratings. Details for the criteria used for scoring can be found in our supplementary material.

5.4. PETAR-Bench

To facilitate standardized and reproducible evaluation, we introduce **PETAR-Bench**—a large-scale benchmark comprising 1,170 lesions and their corresponding PET/CT findings. It includes ground-truth findings, corresponding le-

sion masks, and cross-modality PET/CT data, enabling fine-grained evaluation across linguistic, semantic, and clinical dimensions.

We employ PETAR-Bench to benchmark both 2D and 3D vision—language models under the full set of metrics described above, including human evaluation results. This benchmark establishes the first unified framework for evaluating localized, clinically grounded finding report generation on PET/CT data.

5.5. Main Results

Tab. 3 compares PETAR-4B with a range of 2D and 3D vision—language models across multiple evaluation metrics. Among all models, **PETAR-4B (Ours)** achieves the highest performance across nearly every category, demonstrating its strong capability for localized, clinically coherent report generation from PET/CT volumes.

Compared to the best-performing 2D model, InternVL3, PETAR-4B improves BLEU-4 by 29%, ROUGE-L by 46%, and METEOR by 56%, highlighting the benefit of volumetric reasoning and multimodal fusion. When compared to 3D baselines such as M3D and M3D-RAD, PETAR-4B yields substantial gains in all metrics, most notably in CIDEr (+0.283) and GREEN (+0.175), which measure con-

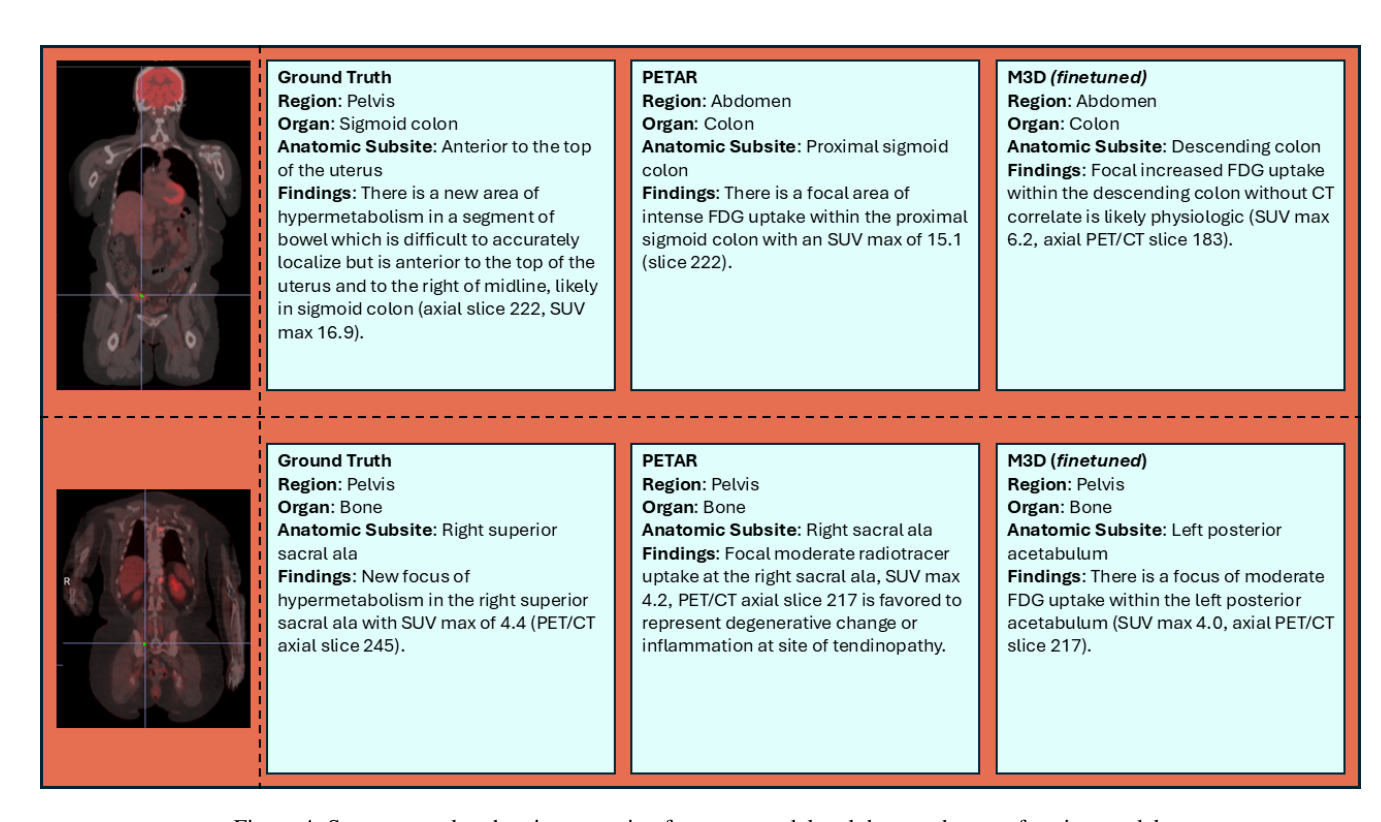


Figure 4. Some examples showing reporting from our model and the next best performing model.

tent diversity and clinical reasoning quality. The model also surpasses the finetuned M3D-RAD baseline, improving BERTScore from 0.7498 to 0.7914 and RaTEScore from 0.6271 to 0.7084, indicating stronger semantic alignment and factual accuracy.

These improvements demonstrate that incorporating mask-aware volumetric conditioning and focal prompting enables PETAR-4B to effectively capture both global anatomical context and fine-grained lesion characteristics, setting a new state of the art in PET/CT report generation.

5.6. Ablation Studies

To assess the contribution of each component in PETAR-4B, we conduct ablation experiments by selectively enabling or disabling the mask input, CT modality, and focal prompt (Tab. 4). The baseline configuration without any of these components performs moderately well, but sequentially adding each module leads to consistent improvements across all metrics.

Introducing the **mask input** improves region-level localization, reflected in gains for CIDEr and RaTEScore, as the model learns to better ground descriptions spatially. Incorporating the **CT modality** further enhances structural understanding and anatomical coherence, yielding higher BERTScore and GREEN. The addition of the **focal prompt** produces the most pronounced gains, boosting CIDEr from

0.1317 to 0.3965 and GREEN from 0.0705 to 0.2260, by allowing the model to focus on small, high-resolution lesion regions.

The full configuration—combining all three components—achieves the best overall results, with peak scores of 0.5312 (BLEU-4), 0.5566 (METEOR), and 0.7084 (RaTEScore). This demonstrates that each component contributes synergistically, and that PETAR-4B's design effectively balances global volumetric reasoning with fine-grained lesion grounding for accurate, clinically meaningful PET/CT report generation.

6. Discussion

The results showed that metrics emphasizing radiologyspecific relevance and semantic similarity correlated most strongly with human judgment, underscoring their clinical validity.

This is just a piece of the PETAR framework. ROIs would be generated by one of a number of existing AI models that have been specifically designed to detect and segment PET lesions for a number of different PET radiotracers. These models would serve as the first stage of PETAR, or, altneratively, physicians can generate ROIs using existing FDA-cleared single-mouse-click PET lesion segmentation tools. In both cases, PETAR would use these ROIs to make critical numerical measurements (size, SUV), and automatically

populate the report with a list of findings and measurements based on the ROIs. We envision the list of findings would then be converted into a templated, free-text report using LLMs, such as automatic impression generators. This remains future work.

7. Conclusion

We introduced **PETAR**, a 3D mask-aware vision–language framework for PET/CT report generation, along with the first large-scale dataset linking lesion-level PET/CT findings to descriptive clinical text. By combining metabolic and structural cues through mask-guided volumetric reasoning and focal prompting, PETAR achieves state-of-the-art performance across linguistic, semantic, and clinically grounded metrics. Our human evaluations further demonstrate strong alignment with expert radiologist judgment, highlighting the model's capacity to produce accurate and clinically useful findings.

8. Acknowledgments

Research reported in this publication was also supported by the National Institute Of Biomedical Imaging And Bioengineering of the National Institutes of Health under Award Number R01EB033782.

References

- [1] Fan Bai, Yuxin Du, Tiejun Huang, Max Q.-H. Meng, and Bo Zhao. M3d: Advancing 3d medical image analysis with multi-modal large language models. *arXiv preprint arXiv:2404.00578*, 2024. 2, 4
- [2] Shruthi Bannur, Kenza Bouzid, Daniel C. Castro, Anton Schwaighofer, Sam Bond-Taylor, Maximilian Ilse, Fernando Pérez-García, Valentina Salvatelli, Harshita Sharma, Felix Meissen, Mercy Ranjit, Shaury Srivastav, Julia Gong, Fabian Falck, Ozan Oktay, Anja Thieme, Matthew P. Lungren, Maria Teodora Wetscherek, Javier Alvarez-Valle, and Stephanie L. Hyland. Maira-2: Grounded radiology report generation. arXiv preprint arXiv:2406.04449, 2024. 2
- [3] Louis Blankemeier, Joseph Paul Cohen, Ashwin Kumar, Dave Van Veen, Syed Jamal Safdar Gardezi, Magdalini Paschali, Zhihong Chen, Jean-Benoit Delbrouck, Eduardo Reis, Cesar Truyts, Christian Bluethgen, Malte Engmann Kjeldskov Jensen, Sophie Ostmeier, Maya Varma, Jeya Maria Jose Valanarasu, Zhongnan Fang, Zepeng Huo, Zaid Nabulsi, Diego Ardila, Wei-Hung Weng, Edson Amaro Junior, Neera Ahuja, Jason Fries, Nigam H. Shah, Andrew Johnston, Robert D. Boutin, Andrew Wentland, Curtis P. Langlotz, Jason Hom, Sergios Gatidis, and Akshay S. Chaudhari. Merlin: A vision language foundation model for 3d computed tomography. arXiv preprint arXiv:2406.06512, 2024. 2
- [4] Mu Cai, Haotian Liu, Siva Karthik Mustikovela, Gregory P. Meyer, Yuning Chai, Dennis Park, and Yong Jae Lee. Vipllava: Making large multimodal models understand arbitrary visual prompts. In *Proceedings of the IEEE/CVF Conference*

- on Computer Vision and Pattern Recognition (CVPR), pages 12914–12923, 2024. 2
- [5] Keqin Chen, Zhao Zhang, Weili Zeng, Richong Zhang, Feng Zhu, and Rui Zhao. Shikra: Unleashing multimodal llm's referential dialogue magic. arXiv preprint arXiv:2306.15195, 2023. 2
- [6] Z. Chen, Y. Bie, H. Jin, and H. Chen. Large language model with region-guided referring and grounding for CT report generation. *IEEE Transactions on Medical Imaging*, 44(8): 3139–3150, 2025. 2
- [7] Ibrahim Ethem Hamamci, Sezgin Er, and Bjoern Menze. Ct2rep: Automated radiology report generation for 3d medical imaging. In Medical Image Computing and Computer Assisted Intervention – MICCAI 2024, 2024. 2
- [8] Hang Hua, Qing Liu, Lingzhi Zhang, Jing Shi, Zhifei Zhang, Yilin Wang, Jianming Zhang, and Jiebo Luo. Finecaption: Compositional image captioning focusing on wherever you want at any granularity, 2024. 2, 4
- [9] Shih-Cheng Huang, Kevin Lee, Kimberly Dodelzon, and et al. Efficiency and quality of generative ai–assisted radiograph reporting. *JAMA Network Open*, 8(10):e2334943, 2025.
- [10] Zachary Huemann, Samuel Church, Joshua D. Warner, Daniel Tran, Xin Tie, Alan B McMillan, Junjie Hu, Steve Y. Cho, Meghan Lubner, and Tyler J. Bradshaw. Vision-language modeling in pet/ct for visual grounding of positive findings, 2025. 3
- [11] Stephanie L. Hyland, Shruthi Bannur, Kenza Bouzid, Daniel Coelho de Castro, Mercy Ranjit, Anton Schwaighofer, Fernando Pérez-García, Valentina Salvatelli, Shaury Srivastav, Anja Thieme, Noel Codella, Matthew P. Lungren, Maria Teodora Wetscherek, Ozan Oktay, and Javier Alvarez-Valle. Maira-1: A specialised large multimodal model for radiology report generation. Technical Report MSR-TR-2023-47, Microsoft Research, 2023. 2
- [12] Chunyuan Li, Cliff Wong, Sheng Zhang, Naoto Usuyama, Haotian Liu, Jianwei Yang, Tristan Naumann, Hoifung Poon, and Jianfeng Gao. Llava-med: Training a large language-andvision assistant for biomedicine in one day. In Advances in Neural Information Processing Systems, 2023. 2
- [13] Long Lian, Yifan Ding, Yunhao Ge, Sifei Liu, Hanzi Mao, Boyi Li, Marco Pavone, Ming-Yu Liu, Trevor Darrell, Adam Yala, and Yin Cui. Describe anything: Detailed localized image and video captioning. In *International Conference on Computer Vision (ICCV)*, 2025. 4
- [14] Zhiliang Peng, Wenhui Wang, Li Dong, Yaru Hao, Shaohan Huang, Shuming Ma, and Furu Wei. Kosmos-2: Grounding multimodal large language models to the world, 2023.
- [15] Zeyi Sun, Ye Fang, Tong Wu, Pan Zhang, Yuhang Zang, Shu Kong, Yuanjun Xiong, Dahua Lin, and Jiaqi Wang. Alphaclip: A clip model focusing on wherever you want. In Proceedings of the IEEE/CVF Conference on Computer Vision and Pattern Recognition (CVPR), pages 13019–13029, 2024.
- [16] Chaoyi Wu, Xiaoman Zhang, Ya Zhang, Yanfeng Wang, and Weidi Xie. Towards generalist foundation model for radiology by leveraging web-scale 2d&3d medical data. arXiv preprint arXiv:2308.02463, 2023. 2

- [17] Yuqian Yuan, Wentong Li, Jian Liu, Dongqi Tang, Xinjie Luo, Chi Qin, Lei Zhang, and Jianke Zhu. Osprey: Pixel understanding with visual instruction tuning. In *Proceedings of the IEEE/CVF Conference on Computer Vision and Pattern Recognition (CVPR)*, pages 28202–28211, 2024. 2
- [18] Shilong Zhang, Peize Sun, Shoufa Chen, Min Xiao, Wenqi Shao, Wenwei Zhang, Kai Chen, and Ping Luo. Gpt4roi: Instruction tuning large language model on region-of-interest. arXiv preprint arXiv:2307.03601, 2023. 2